©ISTOCKPHOTO.COM/RICHCAREY

A Soft Modular End Effector for Underwater Manipulation

A Gentle, Adaptable Grasp for the Ocean Depths

By Domenico Mura, Manuel Barbarossa, Giacomo Dinuzzi, Giorgio Grioli, Andrea Caiti, and Manuel G. Catalano

Current underwater end-effector technology has limits in terms of finesse and versatility. Because of this, the execution of several underwater operations, such as archeological recovery and biological sampling, often still requires direct intervention by human operators, exposing them to the risks of working in a difficult environment. This article proposes the design and implementation of an underactuated and compliant underwater end effector that embodies grasp capabilities comparable to those of a scuba's real hand as well as the large grasping envelope of grippers.

The proposed end effector (Figure 1), with a design based on the Pisa/IIT SoftHand, is composed of a watertight modular chamber with pressure compensation—hosting the electronics and motor—and of a set of two soft terminal devices that implement an adaptive grasping function, one with an anthropomorphic hand form and one with a gripper-like form for medium/small and large object manipulation, respectively. These devices have been tested in a laboratory to withstand a pressure of 50 bar without damage or degradation in performance and are readily interchangeable through a custom fast tool change system.

The two parts are connected via a magnetic drive coupling to transfer actuator torque to the wet fingers. Field results, obtained with the end effector controlled underwater by a human operator (10-m depth), show good grasping performance in terms of both dexterity and force tasks. Moreover, preliminary laboratory testing shows the possibility of implementing basic yet meaningful intrinsic force sensing for the reconstruction of fundamental grasp interactions.

The Difficulties of Underwater Manipulation

Performing fine underwater operations with current robotic manipulation technology is still a very challenging task. In contrast to human divers, atmospheric diving suits (ADSs), remotely operated vehicles (ROVs), and autonomous underwater vehicles (AUVs) can readily and safely access the depths, yet they demonstrate limited manipulation abilities.

Commercially available underwater systems are designed to perform simple and heavy mechanical work (i.e., construction or pipeline maintenance). Generally, they use claw-like end effectors that are capable of opening/closing and wrist-rotation movements only. Such a technological limit means that fine deep-water manipulation tasks are still a goal on the horizon. (For our purposes here, the term *deep water* refers to any sea region that lies beneath diver depth, i.e., approximately 60 m.) This is particularly true for underwater archeological recovery and biological sampling. However, these fields present important tasks, some of which are described later.

Shipwrecks below diver depth present an unusual and more direct insight into ancient cultures. Historical data indicate that the seafloor far offshore contains 20–23% of all wrecks [1], preserved for possibly thousands of years as in a time capsule. Deep near-shore waters, in particular, hold a high number of shipwrecks containing well-preserved artifacts [2]. Biological sampling operations, on the other hand, find a typical application in coral reef studies. Reefs occurring at depths greater than 30 m, which are protected from both human and natural disturbances [3], remain dramatically understudied when compared to other highly diverse habitats. Another example consists of the unexploited biomasses identified in the mesopelagic zone (i.e., the water column between 200 and 1,000 m) [4]. This largely unexplored zone is known to play a significant role in the global carbon cycle, and, if exploited at sustainable levels without impacting biodiversity, this biomass could be used to produce more high-quality ingredients for the human food chain. Biologists work to modify research design, collection methods, and tools to best suit their needs for delicate collection, manipulation, or measurement of deep-sea organisms. The ability to perform these tasks in situ would open up a vast potential for expanding our understanding of sea ecology and of its modifications due to climate change.

Soft robotic hands and grippers appear ideally suited for these kinds of operations: they grasp and manipulate delicate, complex objects by conforming to the object shape and distributing grasping forces. Soft systems also offer improved safety in interactions with humans and animals because of their natural compliance and backdrivability [5]. Among the few underwater robots currently capable of archeological recovery (e.g., the OceanOne by Khatib and colleagues [6], the TRIDENT I-AUV [7], [8], and the MARIS Project AUV [9]) or biological sampling (e.g., [10]), soft grippers are employed for specimen manipulation. However, the richness and complexity of the human hand's sensory and motor functions still remain unmatched by current underwater soft gripper prototypes.

> The richness and complexity of the human hand's sensory and motor functions still remain unmatched by current underwater soft gripper prototypes.

Problem Definition

Underwater archeology consists mainly of locating, monitoring, and preserving archeological sites. Sometimes, however, cultural heritage artifact rescue from such sites becomes crucial, either for preservation or to prevent dispossession. Another typical task is preventive conservation, which aims to prevent or reduce potential damage to artifacts. As with land archeology, recovery and conservation techniques are essentially manual, relying on simple equipment and operator dexterity to handle man-made objects with different shapes, such as jewelry, dishes, weapons, and tools.

In underwater biological sampling, most specimens consist of fragile, soft-bodied organisms, like anemones, sponges, and corals. So scientists need to approach them with the greatest possible care. Regarding, e.g., coral sampling, the most sustainable method is to manually collect loose fragments already broken off from the parent colony or to gently snip a small branch off the parent colony. More complex underwater biological operations consist of tissue biopsy techniques, which use syringes; fluorescence measurements with lamps and lasers; and ribonucleic acid stabilizer application. Some of these tasks are represented in Figure 2(a)–(d). In general, many

Figure 1. The developed system grasping a coin underwater.

other underwater operations require a gentle grasp or working with tools made for the human hand, as in subsea inspection, repair, and maintenance of offshore structure components, e.g., pipelines and umbilicals [see Figure 2(e) and (f)].

The industrial nature of existing underwater robotic manipulation technology does not allow for the performance of such fine activities. Attempts at object grasping often result in damage through the unwitting application of excessive contact forces; this introduces expensive delays or complete failure in task execution. Human skills are still needed and are mostly provided by scuba divers in shallow water or by ADS operators equipped with either unpractical pressurized gloves or primitive lobster-like claws, as shown in Figure 2(g)–(j). These approaches present risks for human life and are highly inefficient.

Proposed Solution

The Pisa/IIT SoftHand [11] is an underactuated, adaptive soft robotic hand that constitutes a flexible-joint robot [14], i.e., its compliance is concentrated in the joints. It is designed to be robust and easy to control as an industrial gripper, while exhibiting high grasping versatility and a form factor similar to that of the human hand. It has 19 joints but needs only one actuator to activate its grasping capabilities. Such simplification is enabled through the theory of adaptive synergies, resulting in a series of considerable advantages both for control and design simplification. The Pisa/IIT SoftHand implements one adaptive synergy, actuated by a transmission system that uses a tendon, pulleys, and a single-gear motor. The SoftHand demonstrates excellent grasping skills in many different situations. In [11], the hand, controlled by a human operator, successfully grasped a total of 107 objects having different shapes. Examples included a bottle, a pen, a cup, a hammer, a book, coins, and so on.

This grasping ability and the soft robotic mechanical design of the SoftHand appear to suit fine underwater operations well, considering in particular the following:

1) The tendon-driven design has already been proven reliable in underwater use (as in [6], inspired by [12]).
2) The SoftHand joints are able to withstand even the severe disarticulations that hydrostatic pressure can create without losing their adaptivity (see, e.g., [11, Fig. 15]).
3) No closed spaces are present in the grasping mechanism, so no pressure differential exists that can cause deformations and ruptures.

Thus, we propose a solution based on the SoftHand technology, i.e., a set of two soft terminal devices, to be used in a waterproof end effector. Such soft devices present

> **Human skills are still needed and are mostly provided by scuba divers in shallow water or by ADS operators equipped with either unpractical pressurized gloves or primitive lobster-like claws.**
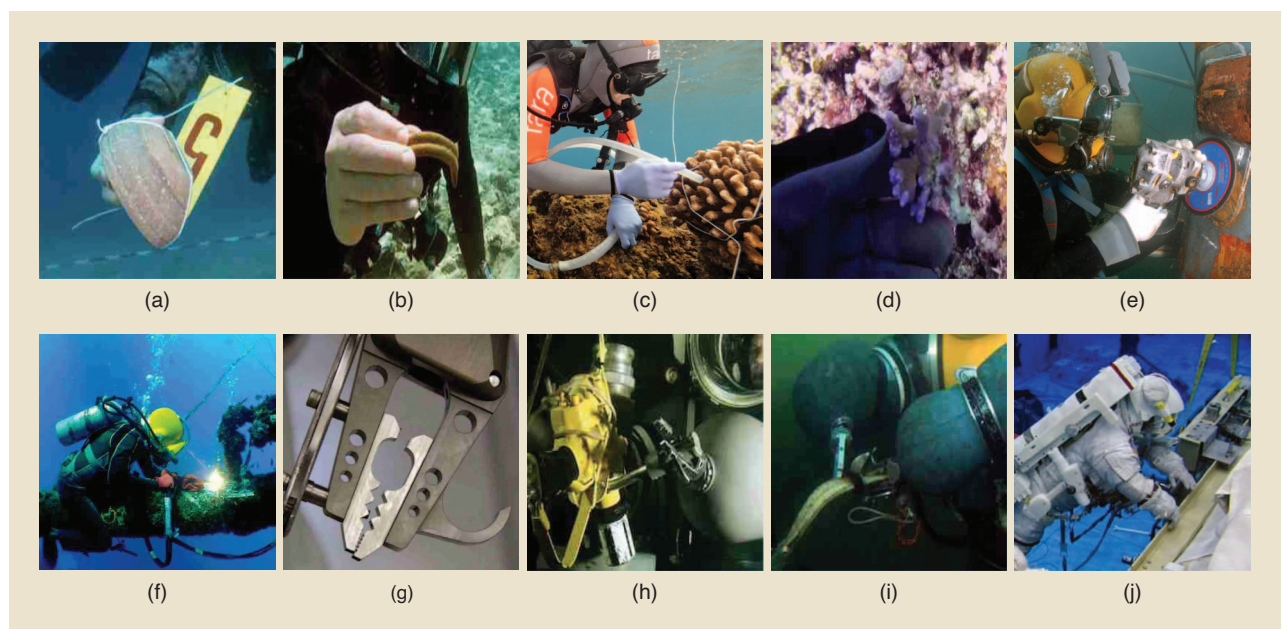
Figure 2. The state of the art in underwater manipulation. Complex postures of the hand performed by scuba divers in (a)–(b) archeological recovery; (c)–(d) biological sampling; and (e)–(f) offshore inspection, repair, and maintenance. (g) A modern ADS pincer-like end effector, (h)–(i) typical deep-water ADS operation, and (j) extravehicular activity conducted underwater with pressurized gloves. [Image (a) is from www.megalehellas.net, image (b) from www.nottingham.ac.uk/archaeology/underwater, image (c) from www.livingoceansfoundation.org, image (d) from www.calacademy.org, image (e) from www.airliquide.com, image (f) from www.antwerpunderwatersolutions.com, image (g) from www.nutyco.com, image (h) from www.oceanworks.com, image (i) from adas.org.au, and image (j) from www.nasa.gov.]

1) the original SoftHand anthropomorphic hand form
2) a gripper-like form with middle phalanges longer than the hand.

The two devices are intended for medium/small and large object grasping. The soft gripper terminal device is designed with an industrial diving scenario in mind. In this environment, it could be used to stabilize an ROV/AUV by firmly catching hold of a structure in a docking procedure. Then, a second robot arm could employ the SoftHand to perform more fine maintenance operations. Finally, more complex underwater manipulation tasks could require an operator/robot to use both developed tools (e.g., if a robot employed in an archeological operation must remove large debris to access smaller artifacts with finesse). So we designed a custom tool change system that enables fast and simple switching between different terminal devices.

Design and Implementation

The design concept, shown in Figure 3(a), is a modular system composed of a waterproof servo-actuator core unit, a set of soft terminal devices readily interchangeable through a tool change system, and an optional waterproof handle device for use by a human operator (e.g., as an ADS end effector). One of the main design issues in submarine operations is electronic waterproofing. Two common techniques are

1) building a water- and pressure-tight enclosure to place electronics
2) encasing all electronics in some resin, a methodology known as *potting*.

We chose the first approach for the core module because it allows easier system modification and intervention. Thus, we designed a watertight enclosure that constitutes the central body of the underwater manipulation system. A section of the complete assembly is presented in Figure 3(b): its maximum diameter is 95 mm, its maximum length 170 mm, and its mass approximately 2 kg. The enclosure components consist of a cast-acrylic tube (7), an O-ring-sealed flange (13), and openings for cable penetrators (14) to allow communication/electrical power supply from the outer environment. To further protect the enclosure from hydrostatic pressure, the hull was filled with mineral oil, thus reducing the pressure excursion between the inner and outer environments.

A second design issue relates to the necessary transmission of the motor torque from inside the watertight enclosure to the outer underwater surrounding, where the wet manipulation system interacts with objects to be grasped. Obtaining a waterproof shaft sealing between those two environments is not trivial: the rotating motion of the shaft can cause momentary pathways for fluids to leak through; with enough pressure/depth, water will eventually penetrate past the seal and into the motor housing. A more reliable solution for this issue is to make the dynamic coupling between the actuated rotor (motor) and the operative rotor immaterial. This is achieved using a magnetically coupled drive consisting of two different sets of magnets: one on the motor side and one on the tool side. Magnetic couplings (MCs) are currently prized for their effectiveness when submerged in water for two main reasons [13], [14]:

1) The technology is intrinsically a torque limiter that can help save the system's electromechanics. The coupling will slip in the case of a severe rupture of the load torque. Moreover, this failure mode can be easily detected through voltage and current monitoring of the motor (see also the section "Fault Detection").
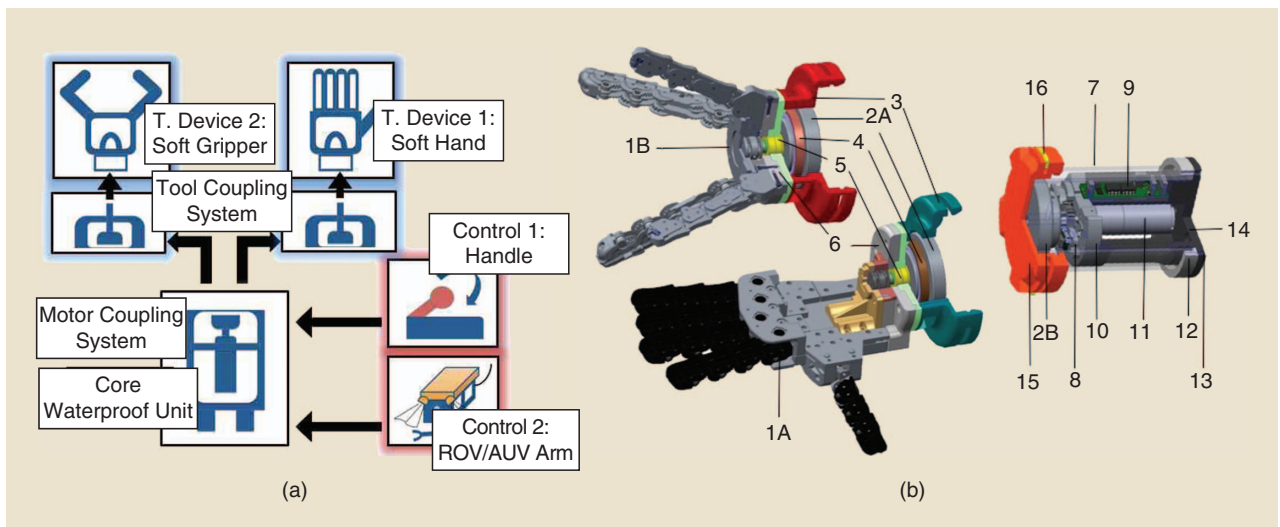

Figure 3. (a) The developed system scheme. The interchangeability of the terminal devices allowed by the MC drive and tool change system is exploited. Tool components are highlighted in blue and control components are in red. (b) The core system and terminal devices sections. The components are numbered as follows: 1A: SoftHand terminal device; 1B: soft gripper terminal device; 2A–2B: inner and outer MC disks; 3: tool coupling device; 4: ferritic stainless steel ring; 5: tool pulley; 6: superior plate; 7: cast-acrylic tube; 8: magnetic encoder group; 9: printed circuit board; 10: central support; 11: motor; 12: inferior flange; 13: inferior end cap; 14: cable penetrator hole; 15: motor-coupling device; and 16: motor-coupling device springs. T.: terminal.

2) The couplings can be manufactured as dust-proof, fluid-proof, and rust-proof and engineered to handle extreme operating conditions.

Even if such a coupling renders the device heavier, this is less relevant in an underwater environment. Considering, thus, the tradeoff between the coupling/device weight and its functionality, the design choice we opted for was a disk-type MC (Magnetic Technologies, http://www.magnetictech.com) capable of transmitting a torque of 1 Nm with a gap between its two plates of about 6 mm (2A and 2B).

The actuator (11) is a 12-Vdc gear Maxon DCX 22 motor with an 83:1 gear ratio. For motor position control, we used two magnetic encoders (8). The encoder magnets are placed on two gears, with a different number of teeth, connected to a third gear mounted on the motor shaft. The combined readings of the two encoders enable the reconstruction of the absolute position of the motor shaft over a range of several turns, thanks to the different gear ratios between the motor and the two sensors. Preliminary experiments proved that neither flooding in mineral oil nor proximity with the coupling magnetic field interferes with the sensors.

The encoders and actuator are connected to the Soft-Hand printed circuit board, which communicates with the outer environment by means of the cables passing though the penetrator. The employed bus carries power/ground and two lines that implement an RS485 communication (see [15] for details).

Thanks to the modular design of the manipulation system and the immaterial coupling provided by the MC, various terminal devices (robotic hands, grippers, and/or tools) can be readily connected to the outer motor shaft using a custom-made tool change system (described in the following section). The developed core system, along with the two terminal devices currently designed, is shown in Figure 3. The maximum lift, pinch grasp, and power grasp forces exerted by the SoftHand are 400, 20, and 76 N, respectively. The lift force value refers to the force that the robotic hand/gripper exerts to hang a corresponding weight, as in Figure 4(c). The gripper's maximum lift force results in about 150 N.

Tool Change System

The tool change system consists, essentially, of a snap mechanism between the motor group and each tool group. Two springs (16) are fastened to the motor group coupling device (15) to realize the snap mechanism, depicted in Figure 5; placing them on the motor group makes a unique motor-coupling mechanism suitable for a set of tools, each equipped with its MC half. The coupling of different tools is rendered fast and simple, thanks to both the MC magnetic attractive force and the spring load, while the uncoupling is possible by means of a custom-made tool housing. Once the motor group is positioned and secured inside the housing, the spring work (i.e., the snap mechanism between the tool and the motor group) is deactivated. In such a configuration, the tool group (3) is fastened to the tool housing, both longitudinally and axially. In particular, the longitudinal fastening is accomplished by a set of magnets that connect to a ferritic stainless-steel ring (4) fastened to the MC half residing in the tool group (2A); the same magnets block the tool MC half, allowing the tool angle of a previously uncoupled tool to be maintained when recoupling with it. The axial fastening makes use of special guides obtained in the tool housing that act as a prismatic joint for the tool group. Thus, the motor group can be uncoupled by the tool group (which remains secured to the tool housing) and retrieved by the operator/robot simply by applying an axial force on it. The coupling/uncoupling procedure is schematically depicted in Figure 5, along with the tool change mechanism configuration in each phase.
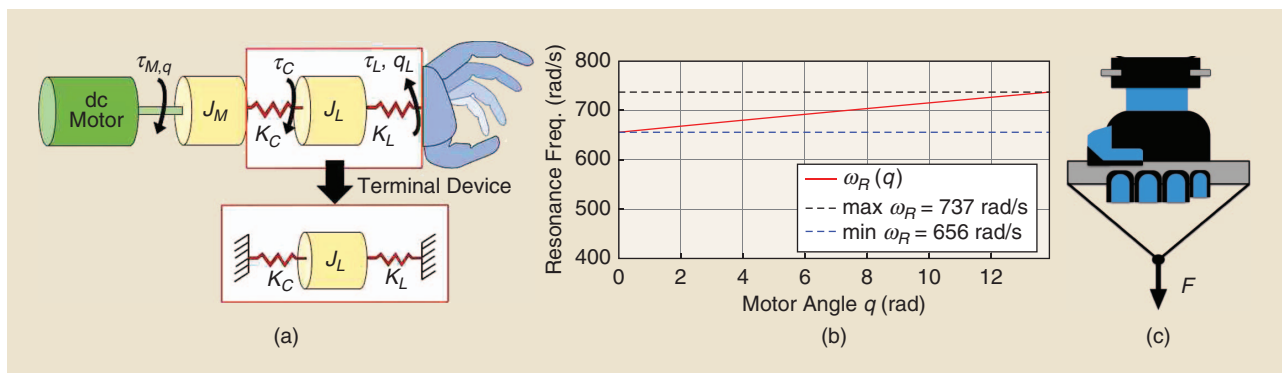
> Laboratory testing assessed the pressure-tolerant nature of the two terminal devices, which were able to withstand a pressure of 50 bar without visible damage or degradation in performance.

Figure 4. (a) A two-inertia representation of the system and analyzed oscillator subsystem. The values J_M and J_L are the combined motor/first coupling half and second coupling half/load inertias, respectively; τ_M, τ_C, and τ_L are the motor, coupling, and load torques, respectively; q and q_L are the motor and load angles, respectively; and K_C and K_L are the coupling and load torsional spring stiffness coefficients, respectively. (b) The resonance frequency $\omega_R(q)$ (in red) of the oscillator of (a) with respect to q. (c) A depiction of the SoftHand terminal device exerting a lifting force equal to F (lift force value definition).
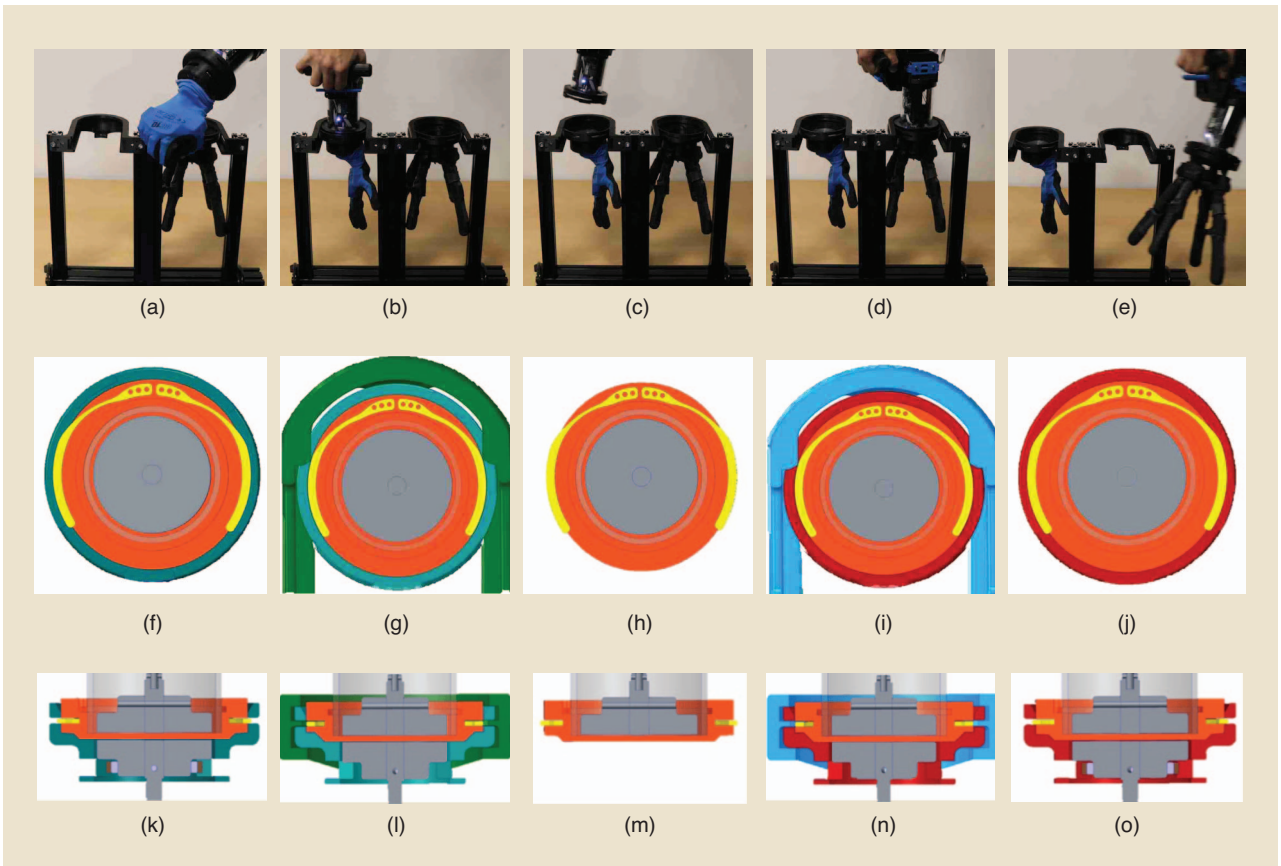
Figure 5. The tool change procedure phases: (a) tool A (the SoftHand), (b) the disengagement, (c) the switch, (d) the engagement, and (e) tool B (the gripper). The respective tool change mechanism configuration in the (f)–(g) longitudinal and (k)–(o) frontal planes. Note the mechanism spring position (in yellow) during the procedure. The springs, tool coupling device, and motor coupling device are depicted with the same colors as in Figure 3(b). The tool change system's flanges are depicted with different colors (light blue and green) to point out their different positions.

MC Control

MCs can be modeled by a two-bodies system (see, e.g., [16]) where, because of a magnetic spring element, a connection exists. Such an elastic element may cause oscillations during position control that could, in turn, degrade control performance. This high-compliance characteristic is known to represent a possible drawback when applied to robot motion control, and it can limit the use of MC to systems with relatively low-bandwidth dynamic transients. Here, we verify that the latter is our case, i.e., the oscillations provided by the MC are negligible.

Consider the representation of our device shown in Figure 4(a), where the recalled two-bodies model has been adopted for the MC. It is important to point out that this is a roughly simplified model: damping or feedback control, obviously present in the real system, are not taken into account. In this manner, we are considering the worst operative conditions. The coupling behaves as a nonlinear soft torsional spring that, if linearized about the origin as in [16], has a stiffness coefficient $K_{C,\mathrm{lin}} = pT_{\max}$, where $p = 10$ is the number of coupling magnetic poles and $T_{\max}$ is its maximum torque. The soft device equivalent stiffness coefficient is nonlinear and depends on the actual motor angle

q. Its linearized expression gives $K_{L,\mathrm{lin}}(q) = K_1 + K_2 q$, where K_1 and K_2 are numerical parameters, previously identified [see (2)]. This varying stiffness coefficient is taken into account in the simplified subsystem, shown in Figure 4(a), which is a harmonic oscillator with an impulse response/transfer function:

$$H(s) = \frac{\Theta(s)}{F(s)} = \frac{1}{J_L} \frac{1}{s^2 + [K_{C,\mathrm{lin}} + K_{L,\mathrm{lin}}(q)]/J_L}. \quad (1)$$

Table 1 shows the numerical values of the quantities defined here. We can evaluate (1) for each $q_0 \leq q \leq q^\star$, where $q_0 = 0$ and $q^\star$ are the motor angles that correspond to an open hand and the hand max closure, respectively. The resonance frequency $\omega_R(q) = \sqrt{[K_{C,\mathrm{lin}} + K_{L,\mathrm{lin}}(q)]/J_L}$ of the function from (1) is computed for increasing values of q, and its trend is shown in Figure 4(b). We can see from the figure that, even in the worst conditions where the damping of the real system is neglected, the lower $\omega_R(q)$ results in $\simeq 650$ rad/s, so employing the motor under this frequency will provide no sensible oscillations in position control. In addition, $\omega_R(q)$ is almost constant, so it can be filtered easily.

Fault Detection

As discussed in the section "Design and Implementation," one of the advantages of drive trains incorporating magnetic gears/couplings is their torque-limiting nature: an excessive torque results in a pole-slipping condition, as opposed to the mechanical damage characteristic of normal gearbox systems. However, from a servo-control perspective, the effect of a magnetic gear pole slipping is a loss of control of the load/tool. Consequently, it is of interest to have a pole-slip detection method.

This can be accomplished by analyzing the absorbed motor current I_m. The algorithm used to identify the pole-slipping condition is based on the grasp force reconstruction algorithm presented in the section "Grasp Force Estimation." This detection could trigger abort/survival modes or initiate a software procedure to automatically reset the motor angular position at rest (q_0) and recover tool functionality.

Pole slipping can be induced even from the tool side of the MC, e.g., if a traumatic event occurs at the terminal device fingers. However, the finger's robust, compliant nature helps in preventing such an event. The robust design of both terminal devices, shown in Figure 6, allows various kinds of finger deformations.

Experimental Results

The developed end effector was validated through both laboratory and field testing; the results are presented next.

Grasp Force Estimation

To aid the operator and/or automated control system of an ROV/AUV, a disturbance observer [17] can be used for grasp force estimation. Consider the following motor dynamic equation:

$$
\begin{aligned}
J_n \ddot{q} = K_{tn} I_{ref} - \tau_d &= K_{tn} I_{ref} - \tau_{model} - \tau_{int} \\
&= K_{tn} I_{ref} - \tau_{model} - \mathbf{J}(q)^T \mathbf{w}_{ext}, \quad (2)
\end{aligned}
$$

where $\ddot{q}$, K_{tn}, I_{ref}, and J_n denote the motor angular acceleration, torque constant, current, and inertia, respectively; $\mathbf{J}(q)$ is the manipulator Jacobian that depends on motor position q; and $\mathbf{w}_{ext}$ represents the wrench exerted by the end effector on the environment (see, e.g., [18]). The disturbance torque τ_d combines all the internal and external disturbance torques and is assumed to be formed by two main components: the torque needed to close the hand τ_{model} when there is no interaction with the environment (i.e., without grasping any object) and the interaction torque τ_{int}.

So the identification procedure aims at obtaining an estimate of τ_{int}, relating it to the current absorbed by the motor. To do so, a calibration procedure is performed to identify the term τ_{model}, which can be decomposed into three components: the elastic torque generated by the hand tendons during closure τ_{te}, the gravitational effect τ_g, and the frictional torque
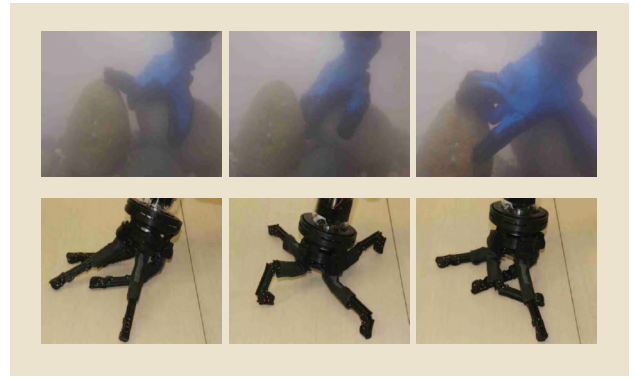

Figure 6. The terminal device deformations against sea stones (top) and a table.

τ_f (mostly due to friction in the actuator gearbox). Considering that τ_g can be mostly neglected, especially for underwater operations, and modeling τ_f with a Hayward-Dahl friction model [19], τ_{model} is defined as

$$
\begin{aligned}
\tau_{model} = D\dot{q} + K_1(q - q_0) + K_2(q - q_0)\|q - q_0\| \\
+ K_f(q - q_f), \quad (3)
\end{aligned}
$$

where q_0 is the motor angular position at rest (hand open), $\dot{q}$ is the motor velocity, D is the viscous damping, K_1 and K_2 are coefficients of a simplified elastic model ($\tau_{te} = K_e(q - q_0) \simeq K_1(q - q_0) + K_2(q - q_0)\|q - q_0\|$), K_f is related to the friction coefficient, and q_f is the adhesion point of the Hayward model.

Assuming that the hand does not come in contact with the object to be grasped [i.e., $\tau_{int} = 0$ in (2)] during the calibration procedure, the hand-model torque can be computed from the motor current and its motion response:

$$
\tau_{model} = K_{tn} I_{ref} - J_n \ddot{q}. \quad (4)
$$

Such a calculation requires motor current and acceleration sensing. The latter would be sensitive to noise if computed from feedback position differentiation, so the equivalent contribution determined by the proportional-integral differential that controls the actuator is computed in feedforward instead.

To identify the parameters of (3), the hand was driven with several velocity reference trajectories from fully open to fully closed and vice versa. Next, the resulting current, position,

Table 1. The numerical values of the parameters given in the section "MC Control."

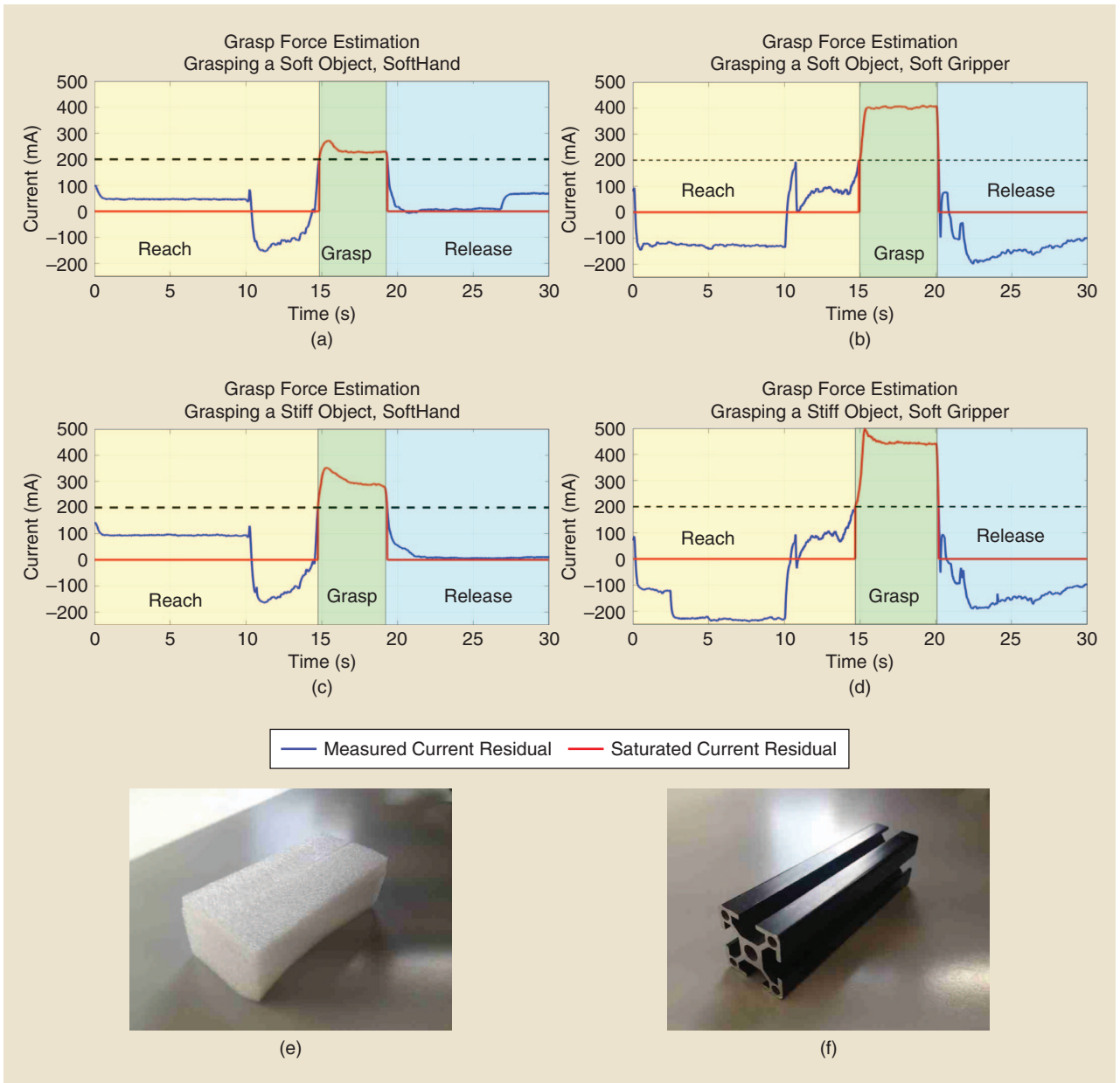| Parameter	Value	Parameter	Value
D	0.7719 mNms	J_n	2.44 Nms²
K_1	0.2619 mNm	$K_{C,lin}$	14 Nm
K_2	0.0002 mNm	J_L	3.25×10^{-4} Nms²
K_f	1,614 mNm	K_{tn}	9.18×10^{-3} Nm/A

Figure 7. (a)–(d) The current residuals obtained during underwater grasping tasks with the (e) soft object and (f) stiff object. Object dimensions are $60\,mm \times 60\,mm \times 120\,mm$. (a)–(c) refer to the SoftHand terminal device; (b)–(d) refer to the soft gripper. Both the measured (in blue) and saturated (for analysis simplification, in red) current residuals are reported. The soft gripper absorbs more current than the SoftHand, by virtue of the former's longer phalanges.

and velocity profiles are used to estimate the parameters (their numerical values are reported in Table 1) by means of conventional least-squares identification algorithm. This leads us to the estimated disturbance torque $\hat{\tau}_{model}$, and the following equality holds:

$$\hat{\tau}_{model} \simeq K_{model} I_{cal}, \qquad (5)$$

where the calibration current I_{cal}, which is the current the motor needs to close the empty terminal device, can now be determined.

Taking I_{cal} as the current offset, experiments in which the hand grasps various objects were carried over. Now, we can establish the following relation:

$$\hat{\tau}_{int} \simeq K_{int} I_{res} \simeq \mathbf{J}(q)^T \mathbf{w}_{ext}, \qquad (6)$$

where $I_{res} = I_m - I_{cal}$ is the current residual measured by the calibrated motor and is recognized as the current the hand needs to close and grasp an object (recall that I_m is the total absorbed motor current); so it is zero if the hand closes empty and proportional to the resistance it encounters

grasping an object, e.g., to the grasped object's stiffness. This behavior is shown in Figure 7. For the same closure reference and object dimension, the current residual is larger when the grasped object is stiffer, denoting a larger interaction force, and reverts to its empty closed-hand value ($\simeq 0$) if the object is pulled out.

To exploit the effects of pole slipping, experiments similar to those presented in the "Laboratory Experiments" section were conducted, applying a load torque demand beyond the capability of the MC (which could happen if an overaggressive control action is applied to the motor). Figure 8 shows the resulting I_m with a dead zone threshold. The excessive load torque occurs when $I_m \simeq 1,500$ mA is applied at $t \simeq 14$ s. As expected, a discontinuity on I_m is observed. Then, the motor position remains constant until $t \simeq 20$ s, when the hand returns to open. Now, however, the I_m results are quite different compared to its open-hand original value (which is set to be $\simeq 0$ mA after a calibration procedure), i.e., before the pole slipping occurred. If we compare Figure 8 with Figure 7, where I_m is shown in the case of successful grasps, it is clear that an uncoupling can be diagnosed through the current monitoring. In this manner, a simple fault-detection algorithm without any sensor on the load side can be implemented.

Laboratory Experiments

To determine an estimate of the end-effector grasping force, laboratory experiments with the estimation algorithm (see the section "Grasp Force Estimation") have been carried out. After calibration, different (stiff or soft) objects are grasped and released by the system inside a water tank. The current residual resulting from these tasks is recorded and reported. An example of the grasp force experiment process and its resulting current residual are presented in Figure 7, where the expected current variations between objects of different stiffness (also shown) can be seen. The experiment is performed for both terminal devices.

A rubber foam block (Young modulus $\simeq 0.015$ GPa) is used as a soft specimen, while a small aluminum bar (Young modulus $\simeq 69$ GPa) represents the stiff specimen. The shape and dimensions of the two objects are very similar. During the grasp phase, the SoftHand yields a mean current residual of $\simeq 250$ mA for the soft object and $\simeq 320$ mA for the stiff one. Regarding the soft gripper, the same quantities result in $\simeq 400$ mA and $\simeq 470$ mA, respectively. As expected, the current residual is proportional to
1) the grasped object's stiffness, i.e., the total grasp force exerted by the end effector
2) the grasp Jacobian of the contact, which is larger for the soft gripper by virtue of its longer middle phalanges.

Moreover, laboratory experiments of the developed fast tool change system have been carried out: a complete tool change procedure is shown in Figure 5.

The manipulation of large objects, difficult to grasp with the SoftHand, has been simulated employing the soft gripper controlled by a human operator. Such tasks are shown in the first two rows of Figure 9.
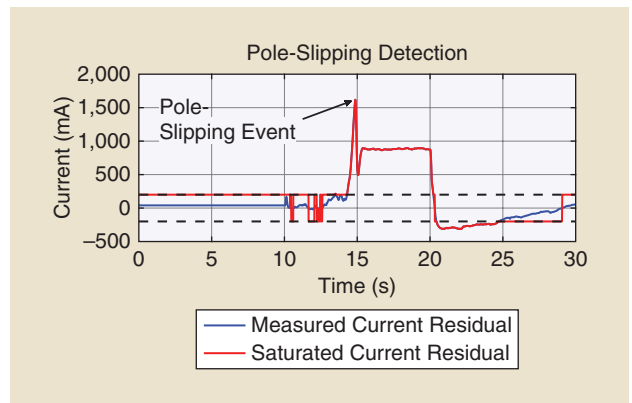

Figure 8. The fault detection experiment with the soft gripper. The excessive motor absorbed current I_m that provokes the pole-slipping condition at $t = 14$ s results in about 1,500 mA. Both the measured (in blue) and saturated (for analysis simplification, in red) motor currents are reported. A saturation threshold of ± 200 mA is depicted as a black dashed line. Compare this figure with Figure 7, where the same experiment is performed without excessive torque demand.

Finally, we performed a pressure test to better assess the pressure-tolerant behavior of our mechanical structure. The two terminal devices underwent a static depth test in a pressure chamber (provided by a company that specializes in underwater robotic research and development, Graal Tech S.r.l. in Genoa, Italy). We inspected them following the test, and they showed no sign of degradation or damage after being subjected to a pressure of 50 bar ($\simeq 500$-m depth). Their performance, too, appeared to be unaffected by the pressure test because, immediately after removing the devices from the chamber, we were able to grasp even complex objects with the SoftHand one (thanks also to the fast tool change system). Video footage of the test is presented in the supplementary material available for this article on IEEE *Xplore*.

Field Experiments

Underwater experimental validation of the system has been carried on at various depths with the two terminal devices depicted in Figure 3. The manipulation system was controlled by a human operator, as in [11]. Figures 9 and 10 present field experiments employing the SoftHand and soft gripper device, respectively, at a depth of $\simeq 1$ m.

In these experiments, focused on the SoftHand terminal device, archeological recovery [Figure 10(a)–(j)] and biological sampling [Figure 10(k)–(t)] operations were simulated, along with a force operation [Figure 10(u)–(y)]. The end effector successfully grasped complex objects like stones, vase shards, coins, reproduced coral pieces, and reproduced aquatic plant

> **The devices' modular nature and the custom tool change system open up the possibility for simple use by an ADS operator or an ROV/AUV robotic arm.**
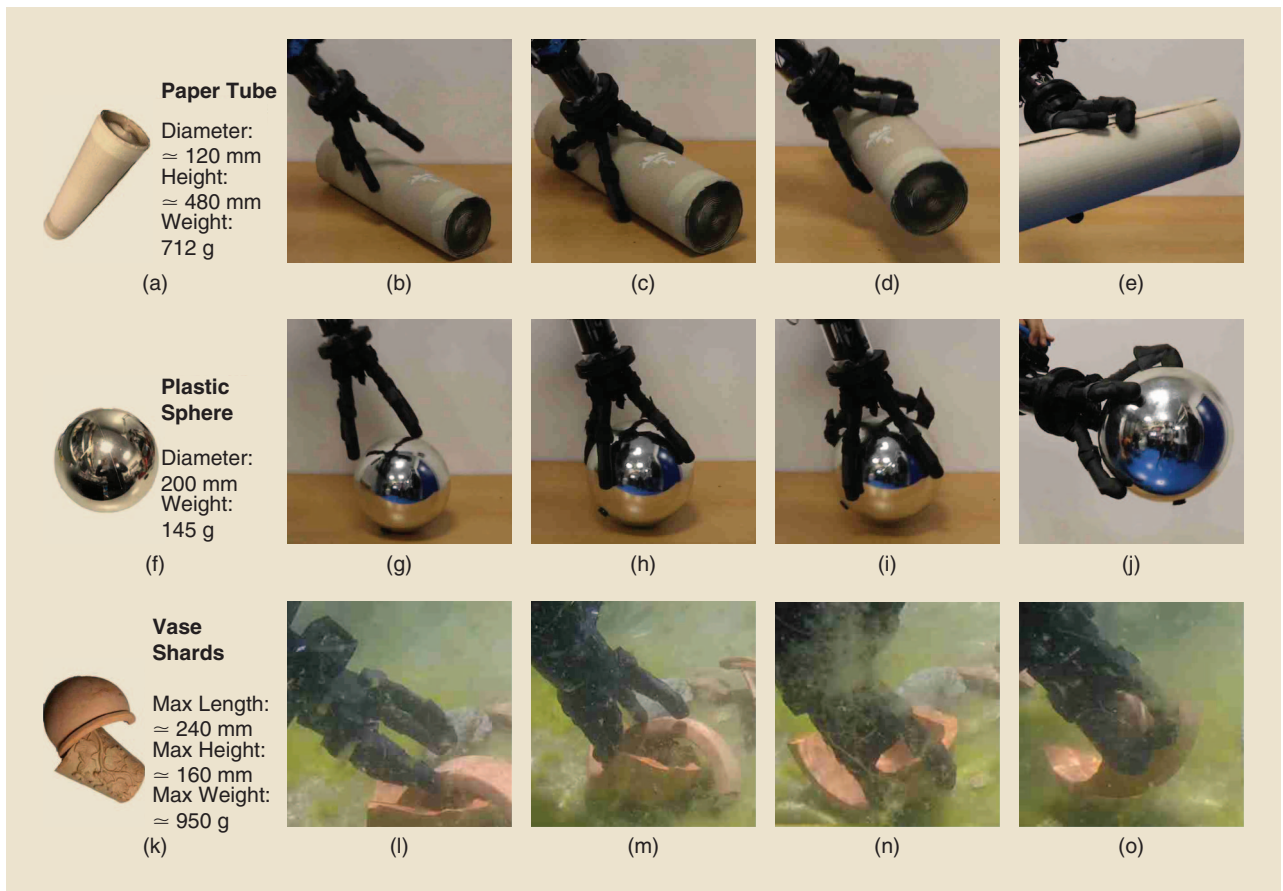
Figure 9. (a)–(o) The validation of the soft gripper terminal device. (a), (f), and (k) show the grasped object's dimensions for every experiment.

stems, with the operator reporting positive feedback about the ease of use. Figure 10 demonstrates that natural, intuitive, and human-like grasping gestures were achieved for every object. In the same field experiments, several grasping tasks were simulated with the soft gripper (as with the SoftHand). Results are shown in Figure 9(k)–(o).

Another field experiment (presented in the multimedia material) took place in the sea near Pisa, Italy (Cecina location), at a depth of $\simeq 10$ m. There, two professional scuba operators employed the SoftHand terminal device via the mechanical handle. They performed several manipulation tasks, similar to those of the 1-m depth experiment. The goal of the experiment was to point out that the manipulation tasks were accomplished with ease by the divers, even though it was the first time they used the device.

Conclusions

In this article, a new underactuated and compliant robotic underwater end effector, based on the technology of the Pisa/IIT SoftHand, was designed and developed. The manipulation system has a modular design that consists of

1) a watertight chamber with pressure compensation, hosting the electronics and motor

2) a set of two soft yet robust terminal devices with the form factor of a SoftHand and of a gripper implementing an adaptive grasping function

3) a custom fast tool change system

4) a mechanical handle for human control of the end effector.

Moreover, the system's terminal devices are readily interchangeable through a magnetic drive coupling that connects the watertight chamber and the two terminal devices, making the dynamic coupling between the actuated-operative rotors immaterial. The devices' modular nature and the custom tool change system open up the possibility for simple use by an ADS operator or an ROV/AUV robotic arm and will, in the future, extend the set of tools that can be mounted by including power tools and the like. A grasping force estimation algorithm was tested with various objects through preliminary laboratory experiments, along with a fault detection procedure. Laboratory testing assessed the pressure-tolerant nature of the two terminal devices, which were able to withstand a pressure of 50 bar without visible damage or degradation in performance. Field results, obtained underwater with a human operator up to a depth of $\simeq 10$ m, demonstrated that this new robotic end effector could be well suited for those operations requiring a fine, adaptable grasp, something that is now challenging
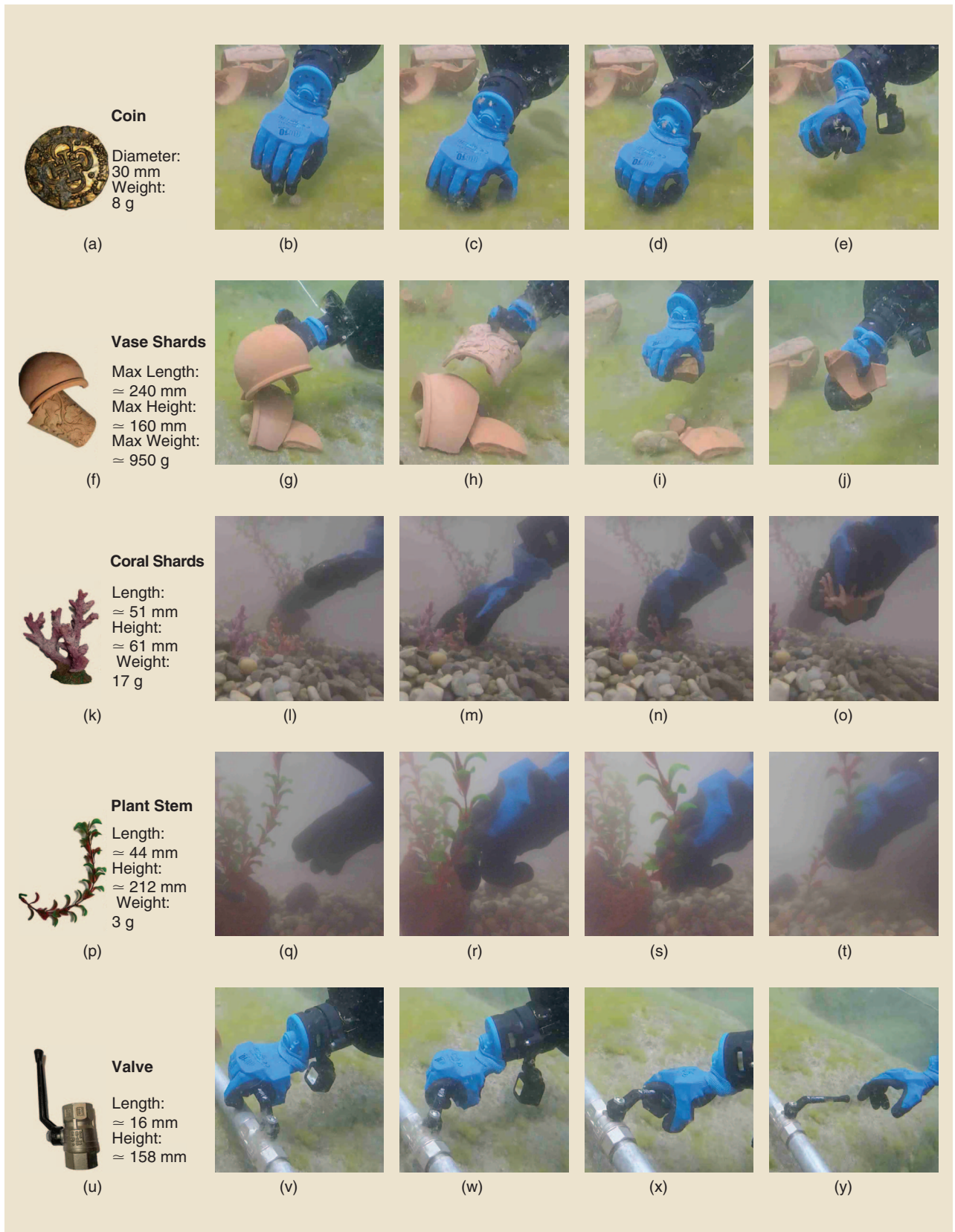
Figure 10. The experimental validation of the end effector with the SoftHand terminal device at a depth of $\simeq 1$ m. The top four rows show dexterous operation, and the bottom row shows a force operation: (a)–(e) archeological recovery, grasping a coin; (f)–(j) archeological recovery, grasping vase shards; (k)–(o) biological sampling, grasping a reproduced coral; (p)–(t) biological sampling, grasping a reproduced aquatic plant stem; and (u)–(y) force operation, turning a valve. (a), (f), (k), (p), and (u) show the grasped object's dimensions for every experiment.

to perform underwater (e.g., archeological recovery and biological sampling). We believe this could aid in the removal of human operators from those underwater tasks, i.e., from the risks of working in such difficult environments.

Acknowledgments

References

[1] B. P. Foley, K. Dellaporta, D. Sakellariou, B. S. Bingham, R. Camilli, R. M. Eustice, D. Evagelistis, V. L. Ferrini, K. Katsaros, D. Kourkoumelis, A. Mallios, P. Micha, D. A. Mindell, C. Roman, H. Singh, D. S. Switzer, and T. Theodoulou, "The 2005 Chios ancient shipwreck survey: New methods for underwater archaeology," *Hesperia*, vol. 78, no. 2, pp. 269–305, 2009.

[2] R. D. Ballard, A. M. McCann, D. Yoerger, L. Whitcomb, D. Mindell, J. Oleson, H. Singh, B. Foley, J. Adams, D. Piechota, and C. Giangrande, "The discovery of ancient history in the deep sea using advanced deep submergence technology," *Deep Sea Res. Part I: Oceanogr. Res. Papers*, vol. 47, no. 9, pp. 1591–1620, 2000.

[3] P. Bongaerts, T. Ridgway, E. Sampayo, and O. Hoegh-Guldberg, "Assessing the 'deep reef refugia' hypothesis: Focus on Caribbean reefs," *Coral Reefs*, vol. 29, no. 2, pp. 309–327, 2010.

[4] C. Robinson, D. K. Steinberg, T. R. Anderson, J. Arístegui, C. A. Carlson, J. R. Frost, J.-F. Ghiglione, S. Hernández-León, G. A. Jackson, R. Koppelmann, B. Quéguiner, O. Ragueneau, F. Rassoulzadegan, Bruce H. Robison, C. Tamburini, T. Tanaka, K. F. Wishner, and J. Zhang, "Mesopelagic zone ecology and biogeochemistry—A synthesis," *Deep Sea Res. Part II: Topical Stud. Oceanogr.*, vol. 57, no. 16, pp. 1504–1518, 2010.

[5] K. Suzumori, "Elastic materials producing compliant robots," *Robot. Autonomous Syst.*, vol. 18, no. 1-2, pp. 135–140, 1996.

[6] H. Stuart, S. Wang, O. Khatib, and M. R. Cutkosky, "The Ocean One hands: An adaptive design for robust marine manipulation," *Int. J. Robot. Res.*, vol. 36, no. 2, pp. 150–166, 2017.

[7] J. Bemfica, C. Melchiorri, L. Moriello, G. Palli, U. Scarcia, and G. Vassura, "Mechatronic design of a three-fingered gripper for underwater applications," *IFAC Proc.*, vol. 46, no. 5, pp. 307–312, 2013.

[8] D. Ribas, P. Ridao, A. Turetta, C. Melchiorri, G. Palli, J. J. Fernández, and P. J. Sanz, "I-AUV mechatronics integration for the trident fp7 project," *IEEE/ASME Trans. Mechatronics*, vol. 20, no. 5, pp. 2583–2592, 2015.

[9] E. Simetti, F. Wanderlingh, S. Torelli, M. Bibuli, A. Odetti, G. Bruzzone, D. L. Rizzini, J. Aleotti, G. Palli, L. Moriello, and U. Scarcia, "Autonomous underwater intervention: Experimental results of the MARIS project," *IEEE J. Ocean. Eng.*, vol. 43, no. 3, pp. 620–639, 2018.

[10] K. C. Galloway, K. P. Becker, B. Phillips, J. Kirby, S. Licht, D. Tchernov, R. J. Wood, and D. F. Gruber, "Soft robotic grippers for biological sampling on deep reefs," *Soft Robot.*, vol. 3, no. 1, pp. 23–33, 2016.

[11] M. G. Catalano, G. Grioli, E. Farnioli, A. Serio, C. Piazza, and A. Bicchi, "Adaptive synergies for the design and control of the Pisa/IIT SoftHand," *Int. J. Robot. Res.*, vol. 33, no. 5, pp. 768–782, 2014.

[12] H. Stuart, S. Wang, B. Gardineer, D. L. Christensen, D. M. Aukes, and M. R. Cutkosky, "A compliant underactuated hand with suction flow for underwater mobile manipulation," in *Proc. 2014 IEEE Int. Conf. Robotics and Automation (ICRA)*, 2014, pp. 6691–6697.

[13] O. Chocron and H. Mangel, "Reconfigurable magnetic-coupling thrusters for agile AUVs," in *Proc. IEEE/RSJ Int. Conf. Intelligent Robots and Systems*, 2008, pp. 3172–3177.

[14] O. Chocron, U. Prieur, and L. Pino, "A validated feasibility prototype for AUV reconfigurable magnetic coupling thruster," *IEEE/ASME Trans. Mechatronics*, vol. 19, no. 2, pp. 642–650, 2014.

[15] C. Della Santina, C. Piazza, G. M. Gasparri, M. Bonilla, M. G. Catalano, G. Grioli, M. Garabini, and A. Bicchi, "The quest for natural machine motion: An open platform to fast-prototyping articulated soft robots," *IEEE Robot. Autom. Mag.*, vol. 24, no. 1, pp. 48–56, 2017.

[16] R. Montague, C. Bingham, and K. Atallah, "Characterisation and modelling of magnetic couplings and gears for servo control systems," in *Proc. IEEE 5th IET Int. Conf. Power Electronics, Machines and Drives*, 2010, pp. 1–6.

[17] M. Nakao, K. Ohnishi, and K. Miyachi, "A robust decentralized joint control based on interference estimation," in *Proc. 1987 IEEE Int. Conf. Robotics and Automation*, 1987, pp. 326–331.

[18] B. Siciliano, L. Sciavicco, L. Villani, and G. Oriolo, *Robotics: Modelling, Planning and Control*, vol. 26, *Series on Advanced Textbooks in Control and Signal Processing*, New York: Springer, 2009, p. 29.

[19] V. Hayward and B. Armstrong, "A new computational model of friction applied to haptic rendering," in *Proc. 1999 Sixth Int. Symp. Experimental Robotics,* pp. 403–412.

Domenico Mura, Department of Soft Robotics for Human Cooperation and Rehabilitation, Istituto Italiano di Tecnologia, Genoa, Italy. E-mail: domenico.mura87@gmail.com.

Manuel Barbarossa, Department of Soft Robotics for Human Cooperation and Rehabilitation, Istituto Italiano di Tecnologia, Genoa, Italy. E-mail: Manuel.Barbarossa@iit.it.

Giacomo Dinuzzi, Department of Soft Robotics for Human Cooperation and Rehabilitation, Istituto Italiano di Tecnologia, Genoa, Italy. E-mail: Giacomo.Dinuzzi@iit.it.

Giorgio Grioli, Department of Soft Robotics for Human Cooperation and Rehabilitation, Istituto Italiano di Tecnologia, Genoa, Italy. E-mail: giorgio.grioli@gmail.com.

Andrea Caiti, Centro di Ricerca "E. Piaggio" and Department of Information Engineering, Università di Pisa, Italy. E-mail: andrea.caiti@unipi.it.

Manuel G. Catalano, Department of Soft Robotics for Human Cooperation and Rehabilitation, Istituto Italiano di Tecnologia, Genoa, Italy. E-mail: manuel.catalano at iit.it.